Silicon Photonic Integrated Fano Resonator With Increased Slope Rate for Microwave Signal Processing

Zheng Dai 🆔, Peng Li 🆔, *Student Member, IEEE*, and Jianping Yao 🆔, *Fellow, Optica, Fellow, IEEE*

Abstract—A tunable silicon photonic (SiP) integrated Fano resonator with an increased slope rate for microwave signal processing is proposed, fabricated, and experimentally demonstrated. A grating-based Fabry-Perot (FP) cavity-coupled micro-ring resonator (MRR) joint with a Mach-Zehnder Interferometer (MZI) is used to form the proposed Fano resonator. Since the resonant modes of the FP cavity and the MZI interfere with that of the MRR, a Fano resonator with an ultra-sharp asymmetric line shape is realized. A microheater is placed on top of the MRR to achieve thermal tuning of the Fano resonance frequency. The proposed Fano resonator is fabricated and experimentally evaluated. A high slope rate (SR) of 379.08 dB/nm and an extinction ratio (ER) of 22.97 dB are obtained. Thanks to its ultra-sharp asymmetric line shape, the applications of the proposed Fano resonator for microwave signal processing are discussed and experimentally demonstrated, including instantaneous frequency measurement with an improved resolution of ±0.2 GHz in a 7 GHz frequency measurement range, and optical temporal differentiation with an increased differentiation gain.

Index Terms—Asymmetric line shape, fano resonator, high slope rate, instantaneous frequency measurement, optical temporal differentiator, silicon photonics, thermal tunability.

I. INTRODUCTION

FANO resonance is a resonant scattering phenomenon that occurs when a discrete state interferes with a continuum of state [1]. Distinct from a conventional Lorentzian resonance with a symmetric line shape, a Fano resonance exhibits an asymmetric line shape in the transmission spectrum. Because of its sharp asymmetric line shape, a Fano resonator can be used for applications such as high-sensitivity sensing, optical filtering, low power optical switching, optical modulation, and fast-slow light generation [2]–[8]. Numerous techniques have been reported to perform Fano resonances in different material

platforms, such as metallic photonic crystals [9], novel plasmonic nanostructures [10], planar metamaterials [11], and silicon photonics (SiP) [12]–[17]. Due to its compatibility with mature complementary-metal-oxide-semiconductor (CMOS) fabrication techniques, SiP has stimulated worldwide research interest for low cost, high volume, and reliable manufacturing of photonic integrated circuits (PICs). In addition, PICs based on silicon have great potential for heterogenous integration in which multiple material systems are being used for the implementation of active and passive photonic devices as well as analog and digital electronic devices for system on chip applications. Several silicon-based designs have been reported to exhibit Fano resonance. For example, a Fano resonance with a maximum extinction ratio (ER) of 4 dB and a slope rate (SR) of around 10 dB/nm was demonstrated in an integrated silicon Bragg reflector by interfering the light reflected from a Bragg waveguide and that from the end of the waveguide facet [15]. The low ER and SR were due to the low reflection coefficient of the end facet of the Bragg waveguide, which would limit the applications where ultra-sharp and deep line shape are needed.

To solve this problem, whispering-gallery resonators such as micro-ring resonators (MRR) and micro-disk resonators (MDR) are employed to provide the discrete localized state. In [16], a Fano resonance was generated by a grating-based Fabry-Perot (FP) cavity-coupled MRR. The ER and SR of the Fano resonator were measured to be 22.54 dB and 250.4 dB/nm, respectively. The performance was improved significantly. However, the tunability of the Fano resonance was limited to a 90 pm range, which was not suitable for applications where a wide wavelength tunable range is needed.

Thanks to the property of a high thermo-optic coefficient in silicon, a large tunable range of a Fano resonance was achieved by incorporating a metallic microheater on top of an MDR [17]. The proposed Fano resonator was implemented by using an add-drop MDR combined with two waveguides having different lengths at the through and drop ports to form a Mach-Zehnder Interferometer (MZI). The interference between the MDR mode and the MZI mode led to a Fano resonance with an asymmetric line shape. The wavelength of the Fano resonance could be tuned by tuning a direct current (DC) applied to the microheater. The wavelength tunable range of the Fano resonator was 15.97 nm, and the ER and SR were 30.2 dB and 41 dB/nm, respectively. Though the wavelength tunability problem was solved, the SR

was not high enough for applications where a very sharp asymmetric line shape is needed, such as high sensitivity microwave signal processing. Thus, a Fano resonance with an increased SR while maintaining a wide wavelength tunable range is highly needed.

Recently, we have proposed a thermally tunable SiP Fano resonator with an increased SR and preliminary results have been reported in [18]. The work here is a continuation of the work in [18] with more details about the device design, fabrication, characterization, and the applications of the device for microwave signal processing. In the device, an FP cavity formed by two Bragg gratings as two reflectors is coupled to an MRR. Two strip waveguides having different lengths with one connected to the FP cavity and the other are connected to the add port of the MRR, and combined via a Y junction. By controlling the waveguide lengths, the MRR radius, the Bragg grating periods, and the FP cavity length, the wavelength of the MRR resonant mode is located at those of the FP cavity mode and the MZI mode. Due to the coupling between the resonant modes of the FP cavity and the MRR, and the MZI, two Fano resonances are generated at the wavelength of the MRR mode, with higher ER and SR. A microheater is placed on top of the MRR to achieve thermal tuning of the Fano resonance. By tuning the DC current to the microheater, the wavelength of the Fano resonance can be widely tuned. The key advantage of our work is that the design takes into account both ultra-sharp asymmetric line shape and wide wavelength tunable range, making it much flexible with higher performance for microwave signal processing. Measurement results show that the maximum ER and SR of the proposed Fano resonator are 22.97 dB and 379.08 dB/nm, respectively, and the wavelength tunable range is 10 nm. The fabricated Fano resonator is employed for microwave signal processing including instantaneous frequency measurement (IFM) with improved sensitivity and resolution, and optical temporal differentiation with an increased differentiation gain.

II. DESIGN AND FABRICATION

The fundamental waveguide structure has a width of 500 nm and a height of 220 nm. Fig. 1(a) shows the perspective view of the proposed SiP Fano resonator. Two Bragg gratings are connected to form a FP cavity and it is coupled with an MRR. Two waveguides having different lengths with one connected to the FP resonator and the other with the add port of the MRR, combined via a Y-junction, to form an MZI. It can be observed that one of the bus waveguides of the add-drop MRR is replaced by the FP cavity, making the FP cavity and the MRR being mutually coupled. Since the resonant modes of the FP cavity and that of the MZI both interfere with that of the MRR, two Fano resonances with asymmetric line shapes would occur at the same wavelength, leading to a higher ER and SR. To enable wavelength tuning, a microheater is placed on top of the MRR to achieve a wide range Fano resonance wavelength tuning. The size of the microheater is made relatively small to avoid thermal leaking to the FP cavity. Fig. 1(b) gives the top view of the coupled MRR and the FP cavity. The MRR has a radius of 8100 nm, and the coupling gap is 170 nm. The corrugation width of
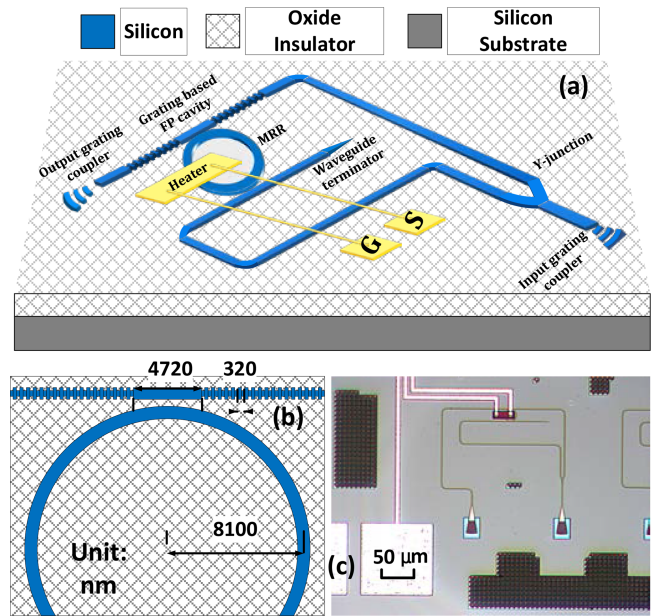
Fig. 1. (a) Schematic of the SiP Fano resonator. (b) Zoom-in view of the grating-based FP cavity-coupled MRR. (c) Microscope image of the device.

the two Bragg gratings is 35 nm and the grating period is 320 nm with a duty cycle of 50%. The FP cavity length is chosen to be 4720 nm to ensure that the grating-based FP cavity resonant at 1540 nm. The length difference between the upper arm and the lower arm of the MZI is designed to be 70 μm, corresponding to a free spectral range of 12.9 nm. The Fano resonator is fabricated with 193-nm deep ultraviolet lithography by AMF, Singapore. Fig. 1(c) shows the microscope image of the fabricated device.

We first use the transfer function method to simulate the transmission response of the proposed Fano resonator [19]–[20]. The whole transmission of this system can be divided into two parts, one is transferred from the pass-through route of the MRR, and the other is from the add port to the drop port of the MRR. This composite system can be modeled as two four-port elements whose scattering properties can be described by two 2×2 matrices, M1 and M2, relating the output fields to the input fields,

$$
\begin{pmatrix} a_{o1} \\ b_{o1} \end{pmatrix} = M_1 \begin{pmatrix} a_{i1} \\ b_{i1} \end{pmatrix}
$$
$$
\begin{pmatrix} a_{o2} \\ b_{o2} \end{pmatrix} = M_2 \begin{pmatrix} a_{i2} \\ b_{i2} \end{pmatrix}
$$
(1)

where a_{i1}, a_{o1}, b_{i1}, b_{o1}, are the input and output electric field amplitudes of the coupled FP cavity and the MRR in the positive and negative positions, a_{i2}, a_{o2}, b_{i2}, b_{o2} are the input and output electric filed amplitudes of the mutually interfered MZI and the MRR in the positive and negative positions, labeled in Fig. 2. Each of the constituent elements (the strip waveguides, the Bragg gratings, and the MRR) can be modeled in scattering matrices, presenting as M_{Li} $(i = 1, 2, 3)$, M_G, and M_{WGMn} $(n = 1, 2)$,

Fig. 2. Top view of the proposed Fano resonator.

given by

$$M_{Li} = \begin{bmatrix} \exp(-i\beta L_i - \alpha L_i) & 0 \\ 0 & \exp(i\beta L_i + \alpha L_i) \end{bmatrix} \quad (2a)$$

$$M_G =$$

$$\begin{bmatrix} \cos(sL_G) - i\delta \sinh(sL_G)/s & -i\xi \sinh(sL_G)/s \\ i\xi \sinh(sL_G)/s & \cos(sL_G) + i\delta \sinh(sL_G)/s \end{bmatrix} \quad (2b)$$

$$M_{WGMn} = \begin{bmatrix} t_{Rn} & 0 \\ 0 & 1/t_{Rn} \end{bmatrix}$$

$$t_{R1} = \frac{\sqrt{1-\kappa^2}\exp(i\beta'2\pi R) - \sqrt{\exp(-\alpha 2\pi R)}}{\exp(i\beta'2\pi R) - \sqrt{1-\kappa^2}\sqrt{\exp(-\alpha 2\pi R)}} \quad (2c)$$

$$t_{R2} = \frac{-\kappa^*\kappa \exp(i\beta'\pi R)\sqrt[4]{\exp(-\alpha 2\pi R)}}{1 - \sqrt{\exp(-\alpha 2\pi R)}t^*t \exp(i\beta'2\pi R)}$$

In (2a), L_i is the length of the strip waveguides, α is the power attenuation of unit length, $\beta = 2\pi n_{eff}/\lambda$ is the propagation constant, where n_{eff} is the effective refraction index, λ is the wavelength of light in vacuum. In (2b), $\delta = \beta - \pi/\Lambda$, $\xi = \Delta n\pi/\lambda$, and $s = \sqrt{\xi^2 - \delta^2}$, where Λ is the Bragg grating period, and Δn is the effective index contrast. In (2c), t_{R1} is the transmission coefficient of the pass-through filter, while t_{R2} is the transmission coefficient of the add-drop filter, κ is the cross-coupling coefficient between the MRR and the waveguides, t is the self-coupling coefficient, β' is the propagation constant of the whispering-gallery mode (WGM) in the MRR, and R is the radius of the MRR. Since $M_1 = M_{L1} M_G M_{L3} M_{WGM1} M_{L3} M_G$, $M_2 = M_{L2} M_{WGM2} M_{L3} M_G$, where L_1 is the length between the upper Y-junction and the pass port of the MRR, L_2 is the length between the lower Y-junction and the add port of the MRR, and L_3 is the half-length of the FP cavity. The amplitude transmission coefficient of each part can be derived from M_1 and M_1, given

Fig. 3. (a) Simulated transmission spectrum of the Fano resonator and measured Fano resonance with the highest ER and SR when a 5-V DC voltage is applied to the device and its zoom-in view. (b) Measured transmission spectrum when the Fano resonator is at the static state. (c) Wavelength tuning of the Fano resonance with the heater power tuned from 0 to 80 mW.

by

$$a_{o1}/a_{i1} = [M_1(1,1)M_1(2,2) - M_1(1,2)M_1(2,1)]/M_1(2,2)$$
$$a_{o2}/a_{i2} = [M_2(1,1)M_2(2,2) - M_2(1,2)M_2(2,1)]/M_2(2,2) \quad (3)$$

A simulation is performed according to the analysis above and the results are shown in Fig. 3(a). In the simulated transmission spectrum, the FP cavity resonant wavelength can be observed in the middle of two wide dips, which is generated by the Bragg grating. Since one of the resonant modes of the MRR is co-located with that of the FP cavity and the MZI (emphasized in the red rectangular box), a Fano resonance with an increased line shape is achieved. In addition, the profile of the Fano resonance can be changed by thermally tuning

the resonant wavelength of the MRR to adjust the wavelength difference between the coupled modes. Furthermore, two extra Fano resonances, in the red elliptical boxes, with lower ERs are shown on the right side, which illustrate the coupling effects that exist between the resonant modes of the MRR and the MZI.

To evaluate the performance of the fabricated SiP Fano resonator, the optical transmission spectrum is measured by using an optical vector network analyzer (LUNA, OVA 5000). The transmission spectrum measured at the output grating coupler is shown in Fig. 3(b), no DC voltage is applied to the microheater. Three periodic Fano resonances with an FSR of 10.8 nm can be observed, which are resulted from the interference between the resonant modes of the MRR and the MZI, and the coupling effects between the MRR and FP cavity modes. Compared with the simulated results in Fig. 3(a), a shift in the resonance wavelength is seen which is caused by the fabrication error. Thanks to the thermal-optic effect in silicon, the resonance wavelength of the MRR can be redshifted by applying a DC voltage to the microheater, which is equivalent to changing the relative resonance wavelength difference between the MRR and the FP cavity, and that of the MRR and the MZI. Thus, a DC voltage (Keithley 2400 Source Meter) is applied to the microheater. When the DV voltage is increased continuously, the wavelength of the Fano resonance is continuously tuned. The results are given in Fig. 3(c), a wavelength shift rate of 91.2 pm/mW is obtained. It is worth noting that the resistance of the microheater is measured to be 50 Ω. To avoid excessive power, an external resistor of 150 Ω is connected in series with the microheater in our experiment. When a 5-V voltage is applied to the microheater, a Fano resonance at 1538.13 nm is observed in Fig. 3(a), which has a maximum SR of 379.08 dB/nm and an ER of 22.97 dB. The zoom-in view of the Fano resonance is also shown in Fig. 3(a). As can be seen, the Fano resonance of the fabricated device is close to that based on simulations, an excellent agreement is achieved. A high insertion loss of around 22 dB is observed in the measured result, which is mostly caused by the low coupling efficiency of the grating couplers. The measurement results also indicate that the proposed device has a 1.51-fold increase in SR compared with the Fano resonator reported in [16] where the SR was 128.68 dB/nm due to the interaction of the resonant modes of the FP cavity and the MZI, both are coupled with that of the MRR.

III. APPLICATIONS FOR MICROWAVE SIGNAL PROCESSING

Thanks to its ultra-sharp asymmetric line shape with high linearity and wide wavelength tuning range, the Fano resonator has a great potential for better-performance microwave signal processing. As two examples, we use the device for two proof-of-concept experiments, including IFM with increased frequency measurement resolution and optical temporal differentiation with an increased differentiation gain.

A. Instantaneous Frequency Measurement

IFM systems play an important role in electronic warfare and intelligence systems and high-resolution sensor systems.
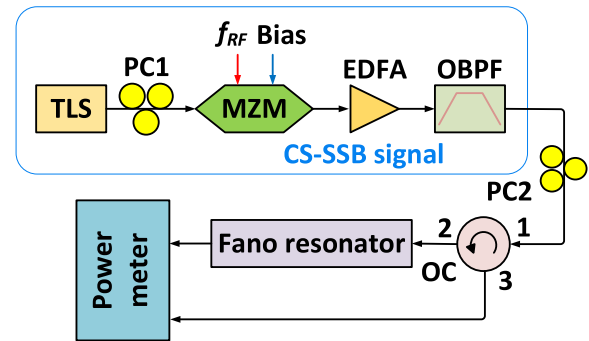
Fig. 4. Schematic diagram of an IFM system by using the SiP Fano resonator. TLS: tunable laser source; PC: polarization controller; MZM: Mach-Zehnder modulator; EDFA: erbium-doped fiber amplifier; OBPF: optical bandpass filter; CS-SSB: carrier suppressed single-sideband; OC: optical circulator.

A traditional electronic IFM RF receiver has limitations of low speed and small bandwidth. Photonics has been introduced as an effective means to realize ultrafast speed and wideband measurements and numerous approaches have been proposed [21]–[27]. One technique is to measure the frequency of a microwave signal based on frequency-to-optical power mapping, in which an amplitude comparison function (ACF) is established. In general, the ACF is the power ratio between two powers at the outputs of two optical filters that have complementary spectral responses. A unique relationship between the power ratio and the frequency to be measured is established. Thus, if the optical power ratio is measured, the frequency of a microwave signal is estimated. However, such a technique generally requires the optical filters with linear spectral responses to guarantee a high measurement accuracy. The proposed Fano resonator has an ultra-sharp asymmetric profile with high linearity, it is a good candidate for high accuracy IFM.

The schematic diagram of the IFM system based on the proposed SiP Fano resonator is shown in Fig. 4. A continuous-wave (CW) light generated by a tunable laser source (TLS) is sent to a Mach-Zehnder modulator (MZM) through a polarization controller (PC1). The light is modulated by a microwave signal at the MZM with its frequency to be measured. The MZM is biased at the minimum transmission point (MITP) to generate a double-sideband with suppressed carrier (DSB-SC) signal. After amplification by an erbium-doped fiber amplifier (EDFA), the signal is sent to an optical bandpass filter (OBPF), to filter out the lower sideband (LSB) to generate a single-sideband with suppressed carrier (SSB-CS) signal. The SSB-CS signal is then sent to the Fano resonator via an optical circulator (OC), with the transmitted and reflected signals sent to a power meter, where the powers of the optical signals are measured. The ACF of the IFM system is given by

$$ACF(\lambda) = \frac{P_T(\lambda)}{P_R(\lambda)} \tag{4}$$

where P_T and P_R are the average powers of the transmitted and reflected optical signals, respectively. Since the frequency of the microwave signal is a function of the ACF, once the value of ACF

is calculated by the measured optical powers, the frequency of the microwave signal is estimated.

An IFM experiment based on the setup shown in Fig. 4 is carried out. A light from the TLS (Yokogawa AQ2201) at 1544.12 nm is sent to the MZM via PC1. A microwave signal generated by a microwave source (Agilent E8254A) with a power of 20 dBm is applied to the MZM via the RF port (20 GHz, JDSU, Model 10026465). By biasing the MZM at the MITP, a DSB-SC signal is generated. After amplified by the EDFA (FiberPrime, EDFA-C-14-S-FA), the CS-DSB optical signal is sent to the OBPF (Finisar, Waveshaper 4000s) to filter out the LSB to get an SSB-CS signal, which is sent to the fabricated Fano resonator via the OC. A temperature controller (TEC, ILX Lightwave LDT-5910B) is used to control the chip temperature at 23 °C. The transmitted and reflected optical signals are sent to the power meter (two-channel, HP 8152A) where the transmitted and reflected optical powers are measured.

The transmission and reflection power spectrum responses of the device when a 9-V DC voltage is applied are shown in Fig. 5(a) and (b), respectively. Fig. 5(c) illustrates the calculated ACF using (4) and the zoom-in view of the linear region is shown in Fig. 5(d). The R-square value is calculated to be 0.9972, confirming that the frequency-to-optical power mapping using the Fano resonance is highly linear, which ensures a high accuracy frequency measurement over the entire measurement range.

The dots in Fig. 6(a) show the microwave frequency measurements for a microwave signal with its frequency tuned from 3 to 10 GHz. The solid line shows the actual ACF of the IFM system. Fig. 6(b) shows the measurement errors. As can be seen, the measurement errors are less than ± 0.2 GHz. In [21], an IFM system using a Fano resonator with a resolution better than ± 0.5 GHz was reported. In the IFM system, the SR of the Fano resonator was 250.4 dB/nm, and the R-square value of the ACF was 0.99. Compared with the IFM system reported in [21], the sensitivity and the resolution of our IFM system are both improved due to the higher SR and the linearity of the Fano resonance profile.

B. Optical Temporal Differentiator

An optical temporal differentiator is an operator that performs temporal differentiation of an arbitrary input signal, which can find applications in pulse characterization [28], pulse shaping [29], and pulse coding [30]. Numerous techniques have been reported to achieve temporal differentiators, such as using a π-phase shifted fiber Bragg grating [31], a tilted fiber Bragg grating [32], or a micro-ring resonator [33]–[34].

Thanks to the large slope rate of the Fano resonator, its use for temporal differentiation can provide a high differentiation gain. Fig. 7 shows an experimental setup for temporal differentiation using the Fano resonator. As can be seen, a pulse from an arbitrary waveform generator (AWG) is applied to a PM.

The electrical field of a light after phase modulations by a signal $s(t)$ is given by [35]

$$e_{PM}(t) = \exp[j\omega_c t + j\beta_{PM}s(t)] \qquad (5)$$
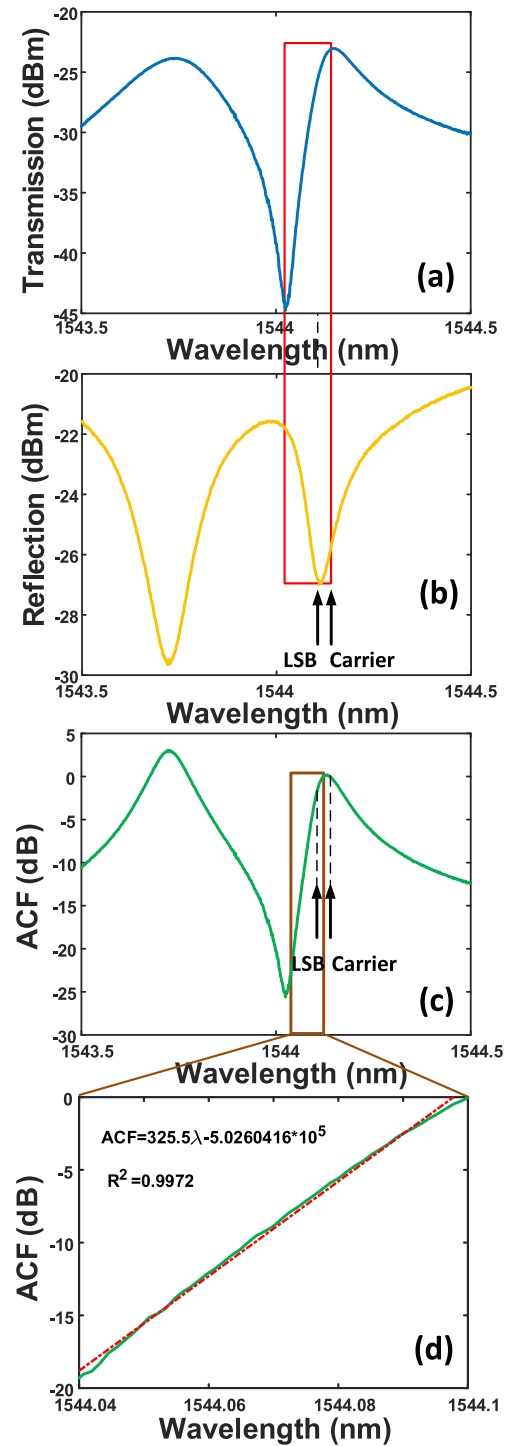
Fig. 5. (a) Transmission spectral response, and (b) reflection spectral response of the proposed Fano resonator when a 9-V DC voltage is applied to the device. (c) the ACF, and (d) a zoom-in view of the linear region of the ACF (solid line) with linear fitting (dotted line). LSB: lower sideband.

where ω_C is the angular frequency of the optical carrier and β_{PM} is the phase-modulation index. Then, the phase modulated optical signal is applied to the Fano resonator, which is employed as a linear frequency discriminator. The frequency response of
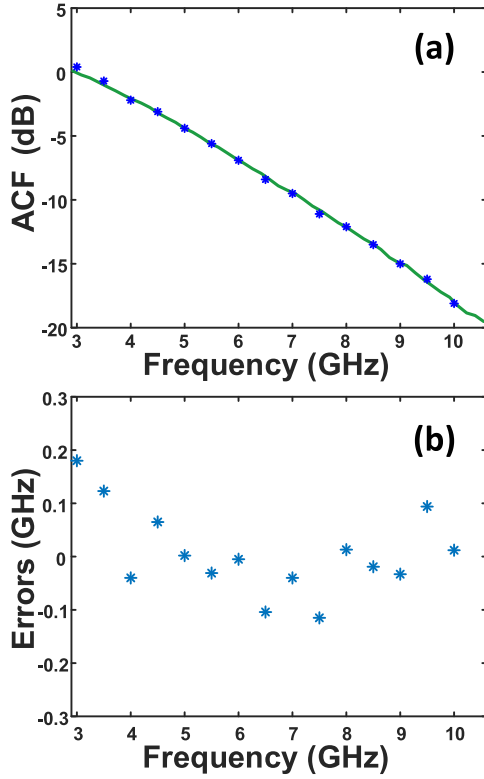
Fig. 6. (a) Microwave frequency measurements when a microwave signal with its frequency tuned from 3 to 10 GHz. (b) Measurement errors.
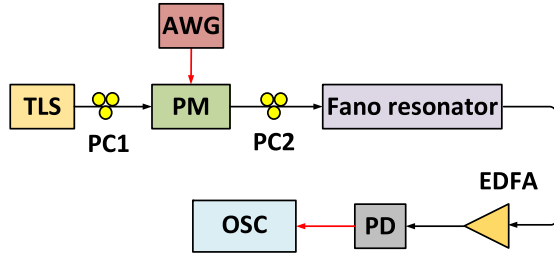
Fig. 7. Schematic diagram of the optical temporal differentiator based on the Fano resonator. TLS: tunable laser source; PC: polarization controller; PM: phase modulator; AWG: arbitrary waveform generator; EDFA: erbium-doped fiber amplifier; PD: photodetector; OSC: oscilloscope.

the frequency discriminator can be expressed by

$$H(\omega) = k(\omega - \omega_0) \tag{6}$$

where k represents the slope rate of the Fano response and ω_0 is the angular frequency when $H(\omega) = 0$. Thus, the output signal in the frequency domain is given by

$$E_{out}(\omega) = k(\omega - \omega_0)E_{PM}(\omega) \tag{7}$$

where $E_{PM}(\omega)$ is the Fourier transform of $e_{PM}(t)$. Applying the inverse Fourier transform to (7), the output signal in the time domain is

$$\begin{aligned} e_{out}(t) &= F^{-1}[k(\omega - \omega_0)E_{PM}(\omega)] \\ &= -jke'_{PM}(t) - k\omega_0 e_{PM}(t) \\ &= [k(\omega_c - \omega_0) + k\beta_{PM}s'(t)]e_{PM}(t) \end{aligned} \tag{8}$$
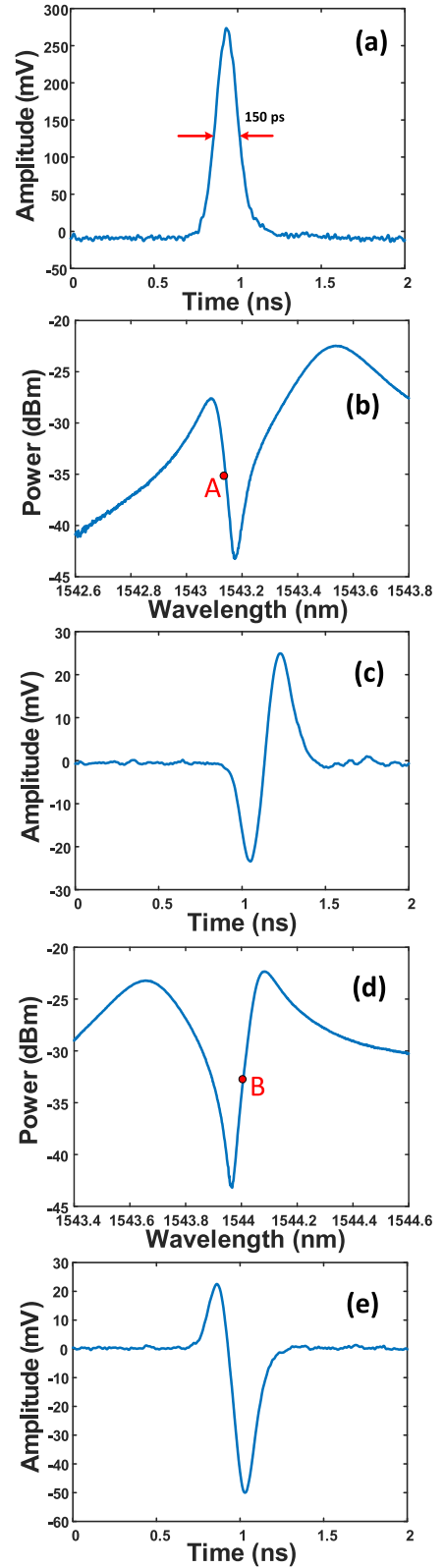
Fig. 8. (a) Waveform of a Gaussian-like input pulse with a temporal width of 150 ps. (b) Transmission spectrum response of the Fano resonator with a negative SR. (c) Waveform of the generated Gaussian monocycle when the optical carrier is located at the point A. (d) Transmission spectrum response of the Fano resonator with a positive SR. (e) Waveform of the generated Gaussian monocycle when the optical carrier is located at the point B.

where $s'(t)$ is the first-order derivative of the input signal $s(t)$. After being detected by a photodetector (PD), the output photocurrent can be expressed by

$$i(t) = 2k^2(\omega_c - \omega_0)\beta_{PM}s'(t) \tag{9}$$

It can be observed that the output signal is proportional to the first-order derivative of the modulating signal. Since the Fano resonator has an ultra-high slope rate k, the temporal differentiator can provide a high differentiation gain.

An experiment is performed based on the setup shown in Fig. 7. Again, a CW light generated by a TLS (Yokogawa AQ2201) is sent to a PM (LN66S-FC) via a PC (PC1), which is modulated by a Gaussian pulse with a temporal width of 150 ps generated by an arbitrary waveform generator (AWG, Keysight M8195A), shown in Fig. 8(a). The phase-modulated optical signal is applied the Fano resonator. After amplification by an EDFA, the optical signal is detected by a PD and the waveform observed by a digital storage oscilloscope (OSC, Keysight DSO-Z 504A).

First, the optical carrier wavelength is tuned at 1543.16 nm, to make it locate at the center of the Fano resonance (point A), as shown in Fig. 8(b). If the optical carrier is modulated by the Gaussian pulse, a monocycle pulse is generated, as shown in Fig. 8(c). That confirms that temporal differentiation is successfully implemented. Then, the optical carrier wavelength is tuned at 1544.04 nm, to make it locate at (point B) the hypotenuse with a positive SR. The generated pulse, which is illustrated in Fig. 8(e), is the inverted version of that shown in Fig. 8(b).

Thanks to the high SR of the Fano resonator, an optical temporal differentiator with a high differentiation gain is achieved.

IV. CONCLUSION

In summary, a tunable SiP Fano resonator with an increased slope rate was proposed and fabricated. In the device, a grating-based FP cavity was coupled to an add-drop MRR. Two stripe waveguides with different lengths were connected to the FP cavity and the add port of the MRR and combined via a Y-junction to form an MZI. Since both FP cavity mode and MZI mode are coupled to that of the MRR, a Fano resonance with an ultra-sharp asymmetric line shape was demonstrated. The tunability of the Fano resonance wavelength was achieved by applying a DC voltage to a microheater, which was placed on top of the MRR. Both ultra-sharp line shape and wide wavelength tuning range were taken into account in our design for microwave signal processing with high performance. A Fano resonance with an ER of 22.97 dB and an SR of 379.08 dB/nm was achieved, and the resonant wavelength tunable range was from 1535 nm to 1545 nm. To evaluate the performance of the proposed Fano resonator, two proof-of-concept experiments were demonstrated, including IFM with an improved resolution and optical temporal differentiation with an increased differentiation gain. Thanks to the ultra-sharp asymmetric line shape with high linearity, the IFM system was demonstrated to have an increased resolution better than ± 0.2 GHz in a frequency measurement range of 7 GHz and

the optical temporal differentiator was demonstrated to have a high differentiation gain due to the high SR of the Fano resonator. Since the proposed Fano resonator combined the ultra-sharp line shape and the wide tunable range, it has shown great potential in enhancing the performance when being used microwave signal processing.

REFERENCES

[1] U. Fano, "Effects of configuration interaction on intensities and phase shifts," *Phys. Rev.*, vol. 124, no. 6, pp. 1866–1878, Dec. 1961.

[2] N. Liu et al., "Plasmonic analogue of electromagnetically induced transparency at the Drude damping limit," *Nature Mater.*, vol. 8, no. 9, pp. 758–762, Jul. 2009.

[3] C. Y. Chen, I. W. Un, N. H. Tai, and T. J. Yen, "Asymmetric coupling between subradiant and superradiant plasmonic resonances and its enhanced sensing performance," *Opt. Exp.*, vol. 17, no. 17, pp. 15372–15380, Aug. 2009.

[4] R. Asadi, M. Malek-Mohammad, and S. Khorasani, "All optical switch based on Fano resonance in metal nanocomposite photonic crystals," *Opt. Commun.*, vol. 284, no. 8, pp. 2230–2235, Apr. 2011.

[5] N. I. Zheludev, S. L. Prosvirnin, N. Papasimakis, and V. A. Fedotov, "Lasing spaser," *Nature Photon.*, vol. 2, no. 6, pp. 351–354, Jun. 2008.

[6] W.-S. Chang et al., "A plasmonic Fano switch," *Nano Lett.*, vol. 12, no. 9, pp. 4977–4982, Sep. 2012.

[7] F. Cheng, B. H. Li, J. Han, H. Xiao, C. Z. Gu, and X. G. Qiu, "Symmetry breaking induced anti-resonance in three dimensional sub-diffraction semiconducting grating," *Appl. Phys. Lett.*, vol. 102, no. 15, Apr. 2013, Art. no. 151113.

[8] Z. L. Samson et al., "Metamaterial electro-optic switch of nanoscale thickness," *Appl. Phys. Lett.*, vol. 96, no. 14, pp. 143103–143105, Apr. 2010.

[9] A. Christ, S. G. Tikhodeev, N. A. Gippius, J. Kuhl, and H. Giessen, "Waveguide-plasmon polaritons: Strong coupling of photonic and electronic resonances in a metallic photonic crystal slab," *Phys. Rev. Lett.*, vol. 91, no. 18, Oct. 2003, Art. no. 183901.

[10] M. Rahmani, B. Luk'yanchuk, and M. Hong, "Fano resonance in novel plasmonic nanostructures," *Laser Photon. Rev.*, vol. 7, no. 3, pp. 329–349, May 2013.

[11] V. A. Fedotov, M. Rose, S. L. Prosvirnin, N. Papasimakis, and N. I. Zheludev, "Sharp trapped-mode resonances in planar metamaterials with a broken structural symmetry," *Phys. Rev. Lett.*, vol. 99, no. 14, Oct. 2007, Art. no. 147401.

[12] A. Bera, M. Kuittinen, S. Honkanen, and M. Roussey, "Silicon slot waveguide Fano resonator," *Opt. Lett.*, vol. 43, no. 15, pp. 3489–3492, Aug. 2018.

[13] Z. Tu, D. Gao, M. Zhang, and D. Zhang, "High-sensitivity complex refractive index sensing based on Fano resonance in the subwavelength grating waveguide micro-ring resonator," *Opt. Exp.*, vol. 25, no. 17, pp. 20911–20922, Aug. 2017.

[14] T. Hu et al., "Tunable Fano resonances based on two-beam interference in microring resonator," *Appl. Phys. Lett.*, vol. 102, no. 1, Jan. 2013, Art. no. 011112.

[15] C.-M. Chang and O. Solgaard, "Fano resonances in integrated silicon Bragg reflectors for sensing applications," *Opt. Exp.*, vol. 21, no. 22, pp. 27209–27218, Nov. 2013.

[16] W. Zhang, W. Li, and J. Yao, "Optically tunable Fano resonance in a grating-based Fabry-Perot cavity-coupled microring resonator on a silicon chip," *Opt. Lett.*, vol. 41, no. 11, pp. 2474–2477, Jun. 2016.

[17] W. Zhang and J. Yao, "Thermally tunable ultracompact Fano resonator on a silicon photonic chip," *Opt. Lett.*, vol. 43, no. 21, pp. 5415–5418, Nov. 2018.

[18] Z. Dai, P. Li, and J. Yao, "SiP Fano resonator with increased slope rate for microwave signal processing," in *Proc. IEEE Int. Topical Meeting Microw. Photon.*, MWP, 2021, pp. 1–4.

[19] W. Liang, L. Yang, J. K. S. Poon, Y. Hung, K. J. Vahala, and A. Yariv, "Transmission characteristics of a Fabry-Perot etalon-microtoroid resonator coupled system," *Opt. Lett.*, vol. 31, no. 4, pp. 510–512, Feb. 2006.

[20] L. Chrostowski and M. Hochberg, "Fundamental building blocks," in *Silicon Photonics Design: From Devices to Systems*. Cambridge, U.K.: Cambridge Univ. Press, 2015, pp. 92–161. doi: 10.1017/CBO9781316084168.005.

[21] B. Zhu, W. Zhang, S. Pan, and J. Yao, "High-sensitivity instantaneous microwave frequency measurement based on a silicon photonic integrated Fano resonator," *J. Lightw. Technol.*, vol. 37, no. 11, pp. 2527–2533, Jun. 2019.

[22] X. Zhang, H. Chi, X. Zhang, S. Zheng, X. Jin, and J. Yao, "Instantaneous microwave frequency measurement using an optical phase modulator," *IEEE Microw. Wireless Compon. Lett.*, vol. 19, no. 6, pp. 422–424, Jun. 2009.

[23] M. Burla, X. Wang, M. Li, L. Chrostowski, and J. Azana, "Wideband dynamic microwave frequency identification system using a low-power ultracompact silicon photonic chip," *Nature Commun.*, vol. 7, no. 1, pp. 1–8, Sep. 2016.

[24] X. Zou, W. Pan, B. Luo, and L. Yan, "Full-scale phase demodulation approach for photonic instantaneous frequency measurement," *Opt. Lett.*, vol. 35, no. 16, pp. 2747–2749, Aug. 2010.

[25] S. Pan, J. Fu, and J. Yao, "Photonic approach to the simultaneous measurement of the frequency, amplitude, pulse width, and time of arrival of a microwave signal," *Opt. Lett.*, vol. 37, no. 1, pp. 7–9, Jan. 2012.

[26] L. Liu et al., "Photonic measurement of microwave frequency using a silicon microdisk resonator," *Opt. Commun.*, vol. 335, pp. 266–270, Jan. 2015.

[27] M. Pagani et al., "Low-error and broadband microwave frequency measurement in a silicon chip," *Optica*, vol. 2, no. 8, pp. 751–756, Aug. 2015.

[28] F. Li, Y. Park, and J. Azana, "Complete temporal pulse characterization based on phase reconstruction using optical ultrafast differentiation (PROUD)," *Opt. Lett.*, vol. 32, no. 22, pp. 3364–3366, Nov. 2007.

[29] J. Yao, F. Zeng, and Q. Wang, "Photonic generation of ultrawideband signals," *IEEE J. Lightw. Technol.*, vol. 25, no. 11, pp. 3219–3235, Nov. 2007.

[30] J. A. N. Silva and M. L. R. Campos, "Spectrally efficient UWB pulse shaping with application in orthogonal PSM," *IEEE Trans. Commun.*, vol. 55, no. 2, pp. 313–322, Feb. 2007.

[31] N. K. Berger, B. Levit, B. Fischer, M. Kulishov, D. V. Plant, and J. Azana, "Temporal differentiation of optical signals using a phase-shifted fiber Bragg grating," *Opt. Exp.*, vol. 15, no. 2, pp. 371–381, Jan. 2007.

[32] M. Li, L. Shao, J. Albert, and J. Yao, "Continuously tunable photonic fractional temporal differentiator based on tilted fiber Bragg grating," *IEEE Photon. Technol. Lett.*, vol. 23, no. 4, pp. 251–253, Feb. 2011.

[33] H. Shahoei, D. Xu, J. Schmid, and J. Yao, " Photonic fractional-order differentiator using an SOI microring resonator with an MMI coupler," *IEEE Photon. Technol. Lett.*, vol. 25, no. 15, pp. 1408–1411, Aug. 2013.

[34] W. Zhang, W. Liu, W. Li, H. Shahoei, and J. Yao, "Independently tunable multichannel fractional-order temporal differentiator based on a silicon-photonic symmetric Mach–Zehnder interferometer incorporating cascaded microring resonators," *IEEE J. Lightw. Technol.*, vol. 33, no. 2, pp. 361–367, Jan. 2015.

[35] J. Yao, F. Zeng, and Q. Wang, "Photonic generation of ultrawideband signals," *IEEE J. Lightw. Technol.*, vol. 25, no. 11, pp. 3219–3235, Nov. 2007.

Zheng Dai received the B.Eng. degree in electrical engineering and automation from Northwestern Polytechnical University, Xi'an, China, in 2015. He is currently working toward the Ph.D. degree in electrical engineering with the Microwave Photonics Research Laboratory, School of Electrical Engineering and Computer Science, University of Ottawa, Ottawa, ON, Canada. His current research interests include parity-time symmetry and its applications in microwave photonics and silicon photonic integrated circuits for microwave signal generation and processing.

Peng Li (Student Member, IEEE) received the B.E. and M.S. degrees from Southwest Jiaotong University, Chengdu, China, in 2011 and 2014, respectively. He is currently working toward the Ph.D. degree with the Center for Information Photonics and Communications, School of Information Science and Technology. From 2019 to 2021, he was a Joint training Ph.D. Student with the Microwave Photonics Research Laboratory, School of Electrical Engineering and Computer Science, University of Ottawa, Ottawa, ON, Canada. His current research interests include microwave photonic signal generation and measurement, radio over fiber, and integrated microwave photonics.

Jianping Yao (Fellow, Optica, Fellow, IEEE) received the Ph.D. degree in electrical engineering from the Université de Toulon et du Var, France, in December 1997. He is currently a Distinguished University Professor and University Research Chair of microwave photonics with the School of Electrical Engineering and Computer Science (EECS), University of Ottawa, Ottawa, ON, Canada. From 1998 to 2001, he was an Assistant Professor with the School of Electrical and Electronic Engineering, Nanyang Technological University (NTU), Singapore. In December 2001, he was an Assistant Professor with the School of Electrical Engineering and Computer Science, University of Ottawa, where he was promoted to an Associate Professor in May 2003, and Full Professor in May 2006. He was appointed University Research Chair of microwave photonics in 2007. In June 2016, he was conferred the title of a Distinguished University Professor of the University of Ottawa. From July 2007 to June 2010 and July 2013 to June 2016, he was the Director of the Ottawa-Carleton Institute for Electrical and Computer Engineering. He has authored or coauthored more than 660 research papers, including more than 380 papers in peer-reviewed journals and more than 280 papers in conference proceedings. Prof. Yao was the Editor-in-Chief of IEEE PHOTONICS TECHNOLOGY LETTERS during 2017–2021, Topical Editor of *Optics Letters* during 2015–2017, an Associate Editor for *Science Bulletin* during 2016–2018, a Steering Committee Member of the *Journal of Lightwave Technology* during 2016–2021, and has been an Advisory Editorial Board Member of *Optics Communications* since 2014. He was the Guest Editor of a Focus Issue on Microwave Photonics in *Optics Express* in 2013, Lead-Editor of a Feature Issue on Microwave Photonics in *Photonics Research* in 2014, and Guest Editor of a special issue on Microwave Photonics in *IEEE/OSA Journal of Lightwave Technology* in 2018. He was the Technical Committee Chair of IEEE MTT-S Microwave Photonics during 2016–2021 and an elected Member of the Board of Governors of the IEEE Photonics Society during 2019–2021. He was a Member of the European Research Council Consolidator Grant Panel in 2016, 2018, and 2020, the Qualitative Evaluation Panel in 2017, and a panelist of the National Science Foundation Career Awards Panel in 2016. He was also the Chair of a number of international conferences, symposia, and workshops, including the Vice Technical Program Committee (TPC) Chair of the 2007 IEEE Topical Meeting on Microwave Photonics, TPC Co-Chair of the 2009 and 2010 Asia-Pacific Microwave Photonics Conference, TPC Chair of the high-speed and broadband wireless technologies subcommittee of the IEEE Radio Wireless Symposium 2009–2012, TPC Chair of the microwave photonics subcommittee of the IEEE Photonics Society Annual Meeting 2009, TPC Chair of the 2010 IEEE Topical Meeting on Microwave Photonics, General Co-Chair of the 2011 IEEE Topical Meeting on Microwave Photonics, TPC Co-Chair of the 2014 IEEE Topical Meetings on Microwave Photonics, General Co-Chair of the 2015 and 2017 IEEE Topical Meeting on Microwave Photonics, and General Chair of the 2019 IEEE Topical Meeting on Microwave Photonics. He was a Committee Member for a number of international conferences, such as IPC, OFC, CLEO, BGPP, and MWP. He was the recipient of the 2005 International Creative Research Award of the University of Ottawa, 2007 George S. Glinski Award for Excellence in Research, and in 2008, he was awarded a Natural Sciences and Engineering Research Council of Canada Discovery Accelerator Supplements Award. Prof. Yao was selected to receive an inaugural OSA Outstanding Reviewer Award in 2012 and was one of the top ten reviewers of the *Journal of Lightwave Technology* during 2015–2016. He was an IEEE MTT-S Distinguished Microwave Lecturer (DML) during 2013–2015 and was the recipient of the 2017–2018 Award for Excellence in Research of the University of Ottawa and the 2018 R.A. Fessenden Silver Medal from IEEE Canada. He is a registered Professional Engineer of Ontario. He was an elected Fellow of the Optica (formerly Optical Society of America) in 2010, Canadian Academy of Engineering in 2012, and Royal Society of Canada in 2018.